Chemical Science

Cite this: *Chem. Sci.*, 2012, **3**, 3421

www.rsc.org/chemicalscience

EDGE ARTICLE

# Mechanistic insight into catalytic oxidations of organic compounds by ruthenium(IV)-oxo complexes with pyridylamine ligands†

**Shingo Ohzu,[a] Tomoya Ishizuka,[a] Yuichirou Hirai,[b] Hua Jiang,[a] Miyuki Sakaguchi,[c] Takashi Ogura,[c] Shunichi Fukuzumi*[bd] and Takahiko Kojima*[a]**

***Received 7th August 2012, Accepted 28th August 2012***
**DOI: 10.1039/c2sc21195e**



A series of Ru(IV)-oxo complexes (**4–6**) were synthesized from the corresponding Ru(II)-aqua complexes (**1–3**) and fully characterized by $^1$H NMR and resonance Raman spectroscopies, and ESI-MS spectrometry. Based on the diamagnetic character confirmed by the $^1$H NMR spectroscopy in $D_2O$, the spin states of **5** and **6** were determined to be $S = 0$ in the $d^4$ configuration, in sharp contrast to that of **4** being in the $S = 1$ spin state. The aqua-complexes **1–3** catalyzed oxidation of alcohols and olefins using $(NH_4)_2[Ce^{IV}(NO_3)_6]$ (CAN) as an electron-transfer oxidant in acidic aqueous solutions. Comparison of the reactivity of electrochemically generated oxo-complexes (**4–6**) was made in the light of kinetic analyses for oxidation of 1-propanol and a water-soluble ethylbenzene derivative. The oxo complexes (**4–6**) exhibited no significant difference in the reactivity for the oxidation reactions, judging from the similar catalytic rates and the activation parameters. The slight difference observed in the reaction rates can be accounted for by the difference in the reduction potentials of the oxo-complexes, but the spin states of the oxo-complexes have hardly affected the reactivity. The activation parameters and the kinetic isotope effects (KIE) observed for the oxidation reactions of methanol indicate that the oxidation reactions of alcohols with the $Ru^{IV}$=O complexes proceed *via* a concerted proton-coupled electron transfer mechanism.

## Introduction

High-valent metal-oxo complexes are one of the most important classes of compounds because of their indispensable roles as reactive intermediates in a number of biological and chemical oxidation reactions.[1–3] Therefore, formation and reactivity of high-valent metal-oxo complexes and the reaction mechanisms have been intensively investigated for decades.[4–10] One of the major procedures to form high-valent metal-oxo complexes is proton-coupled electron-transfer (PCET) oxidation of metal-aqua complexes using water as an oxygen source of the oxo ligand.[11,12] The PCET pathway plays an important role in the oxygen-evolving complex (OEC) in photosystem II.[13,14] OEC consists of a tetranuclear Mn-oxo cluster residing at the reaction center and the cluster catalyzes four-electron oxidation of water to evolve molecular oxygen. It has been proposed that an aqua-ligated manganese site in the cluster is oxidized to generate a $Mn^{V}$=O species *via* a PCET process and the resulting $Mn^{V}$=O species acts as a reactive intermediate to oxidize a water molecule to give molecular oxygen.[13]

Meyer and co-workers have developed catalytic water-oxidation systems using $Ru(OH_2)$-polypyridyl complexes[11] and mechanisms of catalytic water-oxidation systems using $Ru^{V}$=O complexes produced *via* PCET reactions with one-electron oxidants have been extensively studied.[15–18] In addition, $Ru^{IV}$=O complexes, which are formed by PCET oxidations of corresponding Ru(II)-aqua precursor complexes, have also been intensively investigated to gain mechanistic insight into the oxidation reactions of organic substrates.[19] However, as far as we know, few catalytic oxidation systems for organic substrates have been reported, including PCET processes to generate an active metal-oxo species.[12b] Recently, we have reported catalytic oxidation systems, where a PCET oxidant was employed to oxidize $Ru^{II}$–$OH_2$ complexes (**1** and **2**) to form the corresponding reactive $Ru^{IV}$=O complexes (**4** and **5**) and organic substrates such as alcohols and olefins were catalytically oxidized with high efficiency to give a single oxidized product from a substrate.[20,21]

[a]*Department of Chemistry, Graduate School of Pure and Applied Sciences, University of Tsukuba, 1-1-1 Tennoudai, Tsukuba, Ibaraki 305-8571, Japan. E-mail: kojima@chem.tsukuba.ac.jp; Fax: +81-29-853-6503*
[b]*Department of Material and Life Science, Graduate School of Engineering, Osaka University, ALCA, JST, 2-1 Yamada-oka, Suita, Osaka 565-0871, Japan. E-mail: fukuzumi@chem.eng.osaka-u.ac.jp*
[c]*Graduate School of Life Science, University of Hyogo, Kouto, Hyogo 678-1297, Japan*
[d]*Department of Bioinsipired Science (WCU project), Ewha Womans University, Seoul 120-750, South Korea*

† Electronic supplementary information (ESI) available: Synthetic and experimental details, UV-Vis spectral changes, MS, resonance Raman and NMR spectra are included. CCDC 875411. For ESI and crystallographic data in CIF or other electronic format see DOI: 10.1039/c2sc21195e

We report herein a novel $Ru^{II}$–$OH_2$ complex (**3**) with a pentadentate N4Py ligand (N4Py = *N*,*N*-bis(2-pyridyl-methyl)-*N*-bis(2-pyridyl)methylamine)[22] as a candidate for an oxidation catalyst of organic substrates. We have also prepared a new Ru(IV)=O complex (**6**) in an $S = 0$ spin state.[20b] Including the former $Ru^{II}$–$OH_2$ complexes (**1** and **2**), there are available three different precursor complexes with similar ancillary ligands as tris(2-pyridylmethyl)amine (TPA) derivatives. Those precursor complexes can be oxidized to afford corresponding $Ru^{IV}$=O species exhibiting different reduction potentials and different spin states. Therefore, by preparing the three different Ru(IV)=O complexes (**4**–**6** in Fig. 1), we can investigate the details of the influence of difference of spin states of $Ru^{IV}$=O complexes on the reactivity together with mechanistic insights into oxidation of organic substrates on the basis of kinetic analysis. In addition, we examined the effect of the reduction potentials of the active metal-oxo species on the PCET reactivity.

## Results and discussion

### Molecular design and synthesis

Herein, we have prepared three kinds of ruthenium(II)-aqua complexes (**1**–**3** in Fig. 1), which have TPA and its derivatives, 2-(6-carboxyl-pyridyl)methyl-bis(2-pyridylmethyl)amine (6-COOH-TPA)[23] and N4Py as ligands. As we reported previously, the $Ru^{IV}$=O complex with TPA (**4**) was revealed to be in the $S =$ 1 spin state in water,[20a] whereas the $Ru^{IV}$=O complex with 6-$COO^-$-TPA (**5**) showed the unprecedented spin state, $S = 0$, in water.[20b] One of the main reasons that the complex **5** shows such an unusual spin state for $Ru^{IV}$ complexes is the distorted coordination environment of 6-$COO^-$-TPA: the distorted coordination environment allowed the additional coordination of a water molecule to the Ru center to afford a seven-coordinated and pentagonal bipyramidal structure. The coordinated water molecule enabled the complex to form hydrogen bonding between water molecules of the solvent. The seven-coordinate environment has been suggested to stabilize the diamagnetic $S = 0$ spin state of the Ru(IV)-oxo complex compared to the paramagnetic $S = 1$ spin state.[20b] Therefore, we have employed another pentadentate TPA derivative, N4Py, as a ligand in this work to attain a distorted coordination environment[22] for achieving a seven-coordinate structure in water.

The synthesis of a Ru(II)-aqua complex of N4Py, $[Ru^{II}(N4Py)(OH_2)](PF_6)_2$ (**3**), was accomplished by the treatment of $[Ru^{II}Cl(N4Py)](PF_6)$[24] with $AgPF_6$ (Scheme 1). Full characterization of **3** was carried out using $^1$H NMR spectroscopy, ESI-TOF-MS spectrometry, elemental analysis, and X-ray diffraction analysis (*vide infra*). The aqua-complex **3** was oxidized to the Ru(IV)-oxo complex, $[Ru^{IV}(O)(N4Py)(OH_2)](PF_6)_2$ (**6**), with $(NH_4)_2Ce^{IV}(NO_3)_6$ (CAN) as an oxidant. The characterization of **6** was performed by using $^1$H NMR and resonance Raman spectroscopies and also ESI-TOF-MS spectrometry (*vide infra*).

### Crystal structure of 3

A single crystal of **3** suitable for X-ray crystallography was obtained by vapor diffusion of octane into its $CH_2Cl_2$ solution. An ORTEP drawing of the cation part of **3** is depicted in Fig. 2. Complex **3** was crystallized into a monoclinic lattice with the space group of $P2_1/n$: the asymmetric unit consisted of the cationic part of **3**, $[Ru^{II}(N4Py)(OH_2)]^{2+}$, two $PF_6^-$ ions as counter anions, and a $CH_2Cl_2$ molecule as a solvent molecule of crystallization. One of the two $PF_6^-$ ions and a half of the co-crystallized $CH_2Cl_2$ molecule were overlapped on one position by disorder. The bond lengths between the central Ru(II) ion and the pyridine nitrogen atoms of N4Py are in a normal range,[25] however, that of Ru–N1 (tertiary amino nitrogen) is relatively shorter as compared to other Ru–N*x* ($x$ = 2–5) distances: the short bond between Ru and N1 should be derived from the strong σ-donation due to the tertiary amine properties of N1. The bond length of Ru–O1 (2.172(5) Å) was slightly longer than those reported so far for $Ru^{II}$–$OH_2$ (2.10–2.14 Å).[26] The number of counter anions and the bond distances around the Ru center strongly indicate that the oxidation state of the Ru center should be +2. The Ru center was positioned in mean planes consisting of O1–N1–N2–N4 and O1–N1–N3–N5 with deviations from the planes of 0.024 and 0.021 Å, respectively. On the other hand, the Ru center is largely deviated from the mean plane consisting of N2–N3–N4–N5 to the opposite direction of N1 with the distance of 0.263 Å. This deviation was also related to the fact that all the bond angles of N1–Ru–N*x* ($x$ = 2–5) for five-membered chelate rings are smaller than 90° (Table S1 in ESI†) and that the bond angles of N2–Ru–N4 (165.38(18)°) and N3–Ru–N5 (165.14(19)°) are both much smaller than 180°. In addition, a trend was observed that the pyridine rings bonded to the methine carbon of the N4Py ligand (pyridine rings containing N2 and N3) were largely tilted relative to an equatorial plane compared to the

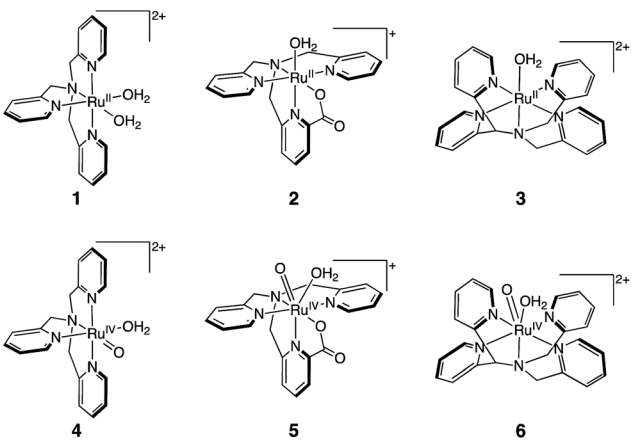


**Fig. 1** Molecular structures of high-valent Ru(IV)=O complexes.

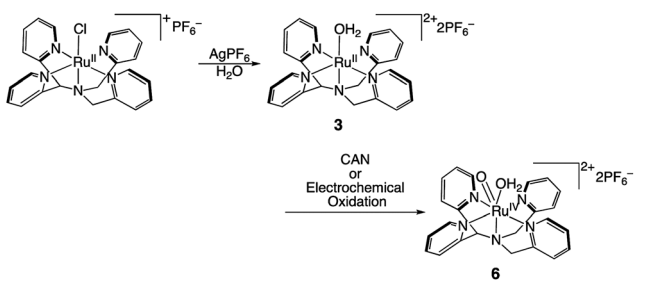


**Scheme 1** Synthesis of $[Ru^{IV}(O)(N4Py)](PF_6)_2$ (**6**).

 

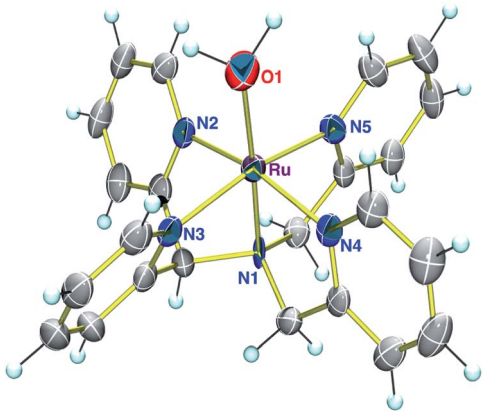


**Fig. 2** Crystal structure of the cation part of **3**. Each atom is described with a thermal ellipsoid at 50% probability. Selected bond lengths (Å): Ru–O1: 2.172(5), Ru–N1: 1.967(5), Ru–N2: 2.057(4), Ru–N3: 2.052(4), 2.061(4), Ru–N5: 2.060(5), and angle (°): O1–Ru–N1: 177.63(18).

pyridine rings bonded to the methylene carbons (pyridine rings containing N4 and N5). The dihedral angles between the O1–N1–N2–N4 plane and the N2- and N4-pyridine rings were 30.5° and 13.5°, respectively, and those between the O1–N1–N3–N5 plane and the N3- and N5-pyridine rings were 51.4° and 12.4°, respectively. The tilting may disturb the efficient π-back donation from the Ru center to the pyridine rings. As a result of the distortion of the coordination environment around the Ru center, the Lewis acidity of the Ru center should increase.

### Spectroscopic and electrochemical characterization of 3

The spectroscopic titration of complex **3** was performed in Britton–Robinson (B.–R.) buffer[27] by addition of a 10 M NaOH aqueous solution using absorption spectroscopy. On the basis of the absorbance changes, the p$K_a$ values of the aqua ligand in **3** were determined as shown in Fig. S1 in the ESI.† The p$K_{a1}$ value for the first deprotonation of the aqua ligand was determined to be 1.85 ± 0.02 and the p$K_{a2}$ value for the deprotonation of the hydroxo-ligand was determined to be 12.0 ± 0.1. The pH-dependent absorption spectral changes were reversible. For comparison, spectroscopic and electrochemical data of the Ru(II)-aqua and Ru(IV)-oxo complexes are summarized in Table 1.

Cyclic and differential-pulse voltammograms (CV and DPV, respectively) of **3** were also measured in B.–R. buffer at various pH values (Fig. S2 in ESI†) and the Pourbaix diagram was drawn based on the results of the electrochemical measurements and the p$K_a$ values obtained (Fig. 3). Above pH 1.8, the aqua ligand of **3** should be deprotonated on the basis of the p$K_{a1}$ value, and thus, the initial state of the complex for the electrochemical measurements is $[Ru^{II}(OH)(N4Py)](PF_6)$ ($Ru^{II}$–$OH^-$). In the Pourbaix diagram, the potential of the first oxidation step is constant to be +0.55 V *vs.* SCE up to pH 2.5, and in the pH range over 2.5, it decreases as the solution pH increases with an inclination of −0.054 V/pH, indicating the $1e^-$ and $1H^+$ process of the $Ru^{II}$–$OH^-$ complex to give $[Ru^{III}(O)(N4Py)]^+$ ($Ru^{III}$–$O^{2-}$). Therefore, the p*K*a value of $[Ru^{III}(OH)(N4Py)]^{2+}$ was estimated to be 2.5. The potential of the second one-electron oxidation step decreased up to pH 2.5 with an inclination of −0.055 V/pH, which was ascribed to a proton-coupled process of $Ru^{III}$–$OH^-$ → $[Ru^{IV}(O)(N4Py)]^{2+}$ ($Ru^{IV}$=O). Above pH 2.5, the second oxidation potential was determined to be constant (+0.87 V *vs.* SCE), independent of the pH value and thus the process can be ascribed to the change from $Ru^{III}$–$O^{2-}$ to $Ru^{IV}$=O. The one-electron reduction potential (+0.90 V *vs.* SCE) of the $Ru^{IV}$=O species at pH 2 is higher than those of **1** (+0.75 V)[20a] and **2** (+0.68 V),[20b] allowing us to expect higher reactivity of **3** for oxidation reactions as compared to those of complexes **1** and **2** (*vide infra*).

Electrochemical oxidation of the aqua complexes **1–3** at +1.3 V (*vs.* SCE) in B.–R. buffer clearly indicated the two-step spectral changes due to generation of the corresponding Ru(III) complexes and the Ru(IV)-oxo complexes with clear isosbestic points (Fig. 4). The reactions were completed in 1 h. In the case of **1**, the electrochemical oxidation for the first 30 min gave rise to the spectral change with two isosbestic points at 565 and 256 nm and a new broad absorption band around 500 nm, as shown in Fig. 4a. For the next 30 min, the isosbestic point was shifted to 294 nm and a new broad band appeared at 410 nm (Fig. S3 in ESI†). As for the complex **2**, the spectral change for the first 30 min proceeded with an isosbestic point at 600 nm to give a new broad absorption at $\lambda_{max}$ = 548 nm as depicted in Fig. 4b. The isosbestic point for the spectral changes of **2** during the next

**Table 1** Summary of the analytical data for **1–3**

| | **1**[d] | **2**[e] | **3** |
|---|---|---|---|
| p$K_{a1}$[a] | 2.1 | 3.5 | 1.85 ± 0.02 |
| p$K_{a2}$[a] | 8.5 | — | 12.0 ± 0.1 |
| $E_{1/2}$ ($Ru^{II/III}$, V *vs.* SCE) at pH 1.8[b] | +0.48 | +0.40 | +0.60 |
| $E_{1/2}$ ($Ru^{III/IV}$, V *vs.* SCE) at pH 1.8[b] | +0.75 | +0.68 | +0.87 |
| $\nu(Ru{=}{}^{16}O)$[c] [$cm^{-1}$] | 806 | 833 | 801 |
| $\nu(Ru{=}{}^{18}O)$[c] [$cm^{-1}$] | 764 | 788 | 761 |
| $\Delta\nu({}^{16}O{-}{}^{18}O)$ [$cm^{-1}$] | 42 | 45 | 40 |

[a] 0.1 M solution in B.–R. buffer titrated with a 10 M NaOH aqueous solution at room temperature. [b] 0.1 mM solution in B.–R. buffer at room temperature; scan rate: 0.1 V $s^{-1}$. [c] Data obtained using resonance Raman spectroscopy. [d] Ref. 20*a*. [e] Ref. 20*b*.

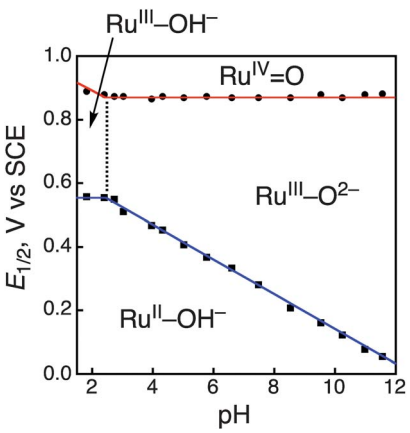


**Fig. 3** A plot of redox potentials against solution pH (Pourbaix diagram) for complex **3** in B.–R. buffer. Potentials were determined relative to SCE (as 0 V) at room temperature. The squares and blue line indicate the $Ru^{II/III}$ couples, and the circles and red line correspond to the $Ru^{III/IV}$ couples.

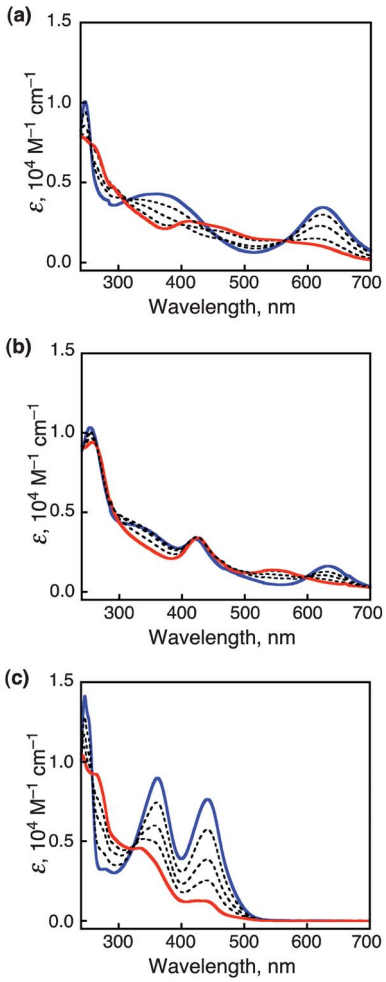


**Fig. 4** Spectral changes every 15 min during the electrochemical oxidation of (a) **1**, (b) **2**, and (c) **3** in B.–R. buffer (pH 1.8; sample concentration, 0.5 mM) at room temperature. The initial spectrum of each complex and the final spectrum are indicated as the blue and red lines, respectively.

30 min was observed at 287 nm (Fig. S3b in ESI†). As the oxidation of **3** proceeded, the MLCT absorption at 440 nm gradually faded and instead a new broad absorption was observed at 260–300 nm (Fig. 4c). For the first 30 min, two isosbestic points appeared at 325 and 258 nm, and during the next 30 min, no isosbestic point was observed within the wavelength range measured. The absorption spectral changes in the course of the electrochemical oxidations of complexes **1–3** ended at the elementary electric charges of 0.198 C for **1**, 0.201 C for **2**, and 0.188 C for **3**, loaded into the solution, which are comparable to the theoretical value for the two-electron oxidation of $Ru^{II}$ species to form the corresponding $Ru^{IV}$ complexes (0.193 C).

The ESI-MS spectrum was measured for the aqueous solution of **6** generated by the oxidation with CAN and a peak cluster was observed at $m/z = 242.56$ with the feature of a divalent cation, which was ascribable to the signal of $[\mathbf{6} - 2PF_6]^{2+}$ (Fig. S4 and S5 in ESI†). When the oxidation of **3** was performed in $H_2{}^{18}O$, the peak cluster was shifted to $m/z = 243.54$, assigned to $^{18}O$-labeled $[Ru^{IV}(^{18}O)(N4Py)]^{2+}$ (calcd 243.54) (Fig. S4b in ESI†) *via* the substitution of the $^{16}O$-aqua ligand with $H_2{}^{18}O$.[28] The ESI-MS spectrum of the complex **6** generated electrochemically displayed the same features as those for the sample obtained by the oxidation of **3** with CAN (Fig. S6 in ESI†).

Resonance Raman spectroscopy suggests the existence of a Ru=O double bond in **6** ($\nu = 801$ cm$^{-1}$) and the Raman scattering band was shifted to $\nu = 761$ cm$^{-1}$ with the use of $H_2{}^{18}O$ in place of $H_2{}^{16}O$ as the solvent for the formation of the Ru(IV)-oxo complex (Fig. S7 in ESI†).[29] The observed isotope shift ($\Delta\nu = 40$ cm$^{-1}$) showed a good agreement with the calculated value ($\Delta\nu = 40$ cm$^{-1}$) for the Ru=O harmonic oscillator.[20] The Raman shift of the $Ru^{IV}$=O bond for **6** is comparable to those of **4** with TPA (806 cm$^{-1}$)[20a] and $[Ru(O)(TPA)(bpy)]^{2+}$ (805 cm$^{-1}$),[30] but lower than that (833 cm$^{-1}$) of **5** with 6-$COO^-$-TPA.[20b]

The $^1$H NMR spectrum of **6** generated by the oxidation of **3** with CAN[31] in $D_2O$ showed well-resolved signals in the range of 3–9 ppm, indicating a diamagnetic character of **6**, and thus the spin state of **6** is obviously $S = 0$ (Fig. 5) at room temperature. In addition, the yield of **6** based on the amount of **3** was nearly quantitative, as estimated by peak integration of the $^1$H NMR signals relative to that of DSS (4,4-dimethyl-4-silapentane-1-sulfonic acid) added as an internal reference. The assignments of the $^1$H NMR signals due to both **3** and **6** were performed with 2D $^1$H–$^1$H COSY and 1D NOE measurements (Fig. S9 and S10 in ESI†). In a comparison of the spectrum of complex **6** in $D_2O$ with that of **3**, most of the $^1$H NMR signals of **6** exhibited downfield shifts due to the higher oxidation state of the Ru(IV) center in **6** than those of **3** with Ru(II), and thus, the Lewis acidity of the Ru center should be enhanced in **6** to exert stronger electron-withdrawing effects on the ligand. Characteristic differences in the $^1$H NMR spectra between **3** and **6** were observed for the signals of 6-Hs of the pyridine rings bonded to the methylene carbon (doublet), the proton of the methine carbon (singlet), and the methylene protons (AB quartet); the shift widths ($\Delta\delta$) for the proton signals from complex **6** to **3** were −0.40, +0.97, +0.95 and +1.24 ppm, respectively. The large downfield shifts of the methine- and methylene-protons may be ascribed to the effect of

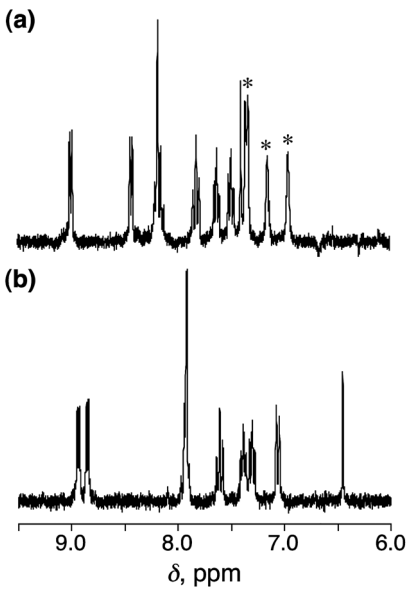


**Fig. 5** $^1$H NMR spectra of complex (a) **6** and (b) **3** in $D_2O$. The asterisks (*) denote signals derived from the ammonium ions of CAN.

 

the increase in the oxidation number at the Ru center as a Lewis acid, affecting most strongly the σ-donating amine nitrogen (N1) of the N4Py ligand through the strong σ-bond between them. The effect of oxidation of the Ru center also strongly influences the electronic states of the carbons adjacent to the amine nitrogen. The upfield shifts of 6-Hs of the pyridine rings bonded to the methylene carbon (N4- and N5-pyridine rings)[32] is probably ascribed to the tilt of the pyridine rings, which is caused by the steric effect of the additional coordination of a water molecule (*vide infra*). As a result of the tilting, the 6-Hs are located on the ring currents of the pyridine rings bonded to the methine carbons (N2- and N3-pyridine rings).

### Origins of the unusual $S = 0$ spin state for $Ru^{IV}$=O species 5 and 6

We have reported that a seven-coordinated pentagonal bipyramidal structure of the Ru center involving an additional aqua ligand derived from the solvent, as suggested by DFT calculations on **5** with 6-$COO^-$-TPA, plays a key role to stabilize the singlet state relative to the triplet state in water.[20b] In the case of **6**, a seven-coordinated structure with a solvent water molecule, as well as in the case of **5**,[20b] is indispensable to stabilize the $S = 0$ state of **6** (Fig. 6), since the coordination environment made of the N4Py ligand is distorted from an ideal octahedron as seen in the crystal structure of **3**. As a result of the seven coordination, the total electron density donated from the ligands in the basal equatorial plane of the pentagonal bipyramid increased, the $d_{xy}$ orbital of the Ru(IV) center is destabilized and the singlet state becomes more favored than the triplet state. Thus the formulation of low-spin **6** should be $[Ru(O)(N4Py)(OH_2)]^{2+}$ in water.

### Catalytic oxidation of organic substrates

By using the Ru(II)-aqua complexes, $[Ru^{II}(TPA)(OH_2)_2](PF_6)_2$ (**1**), $[Ru^{II}(6\text{-}COO\text{-}TPA)(OH_2)](PF_6)$ (**2**) and complex **3**, as catalysts, catalytic oxidation reactions of benzyl alcohol and the *para*-substituted derivatives, aliphatic alcohols (1- and 2-propanols, and methanol), olefins (styrene and cyclohexene) and a water-soluble ethylbenzene derivative were carried out with CAN as an electron-transfer oxidant in $D_2O$ at room temperature. The product yields after stirring for 1 h were determined using $^1H$ NMR spectroscopy (Table 2 and Fig. S11 in ESI†). As control experiments, we examined the reactions of the substrates listed in Table 2 with CAN under the same reaction conditions except in the absence of the catalysts to confirm that the substrates employed were almost intact and persistent against CAN under the reaction conditions.[33]

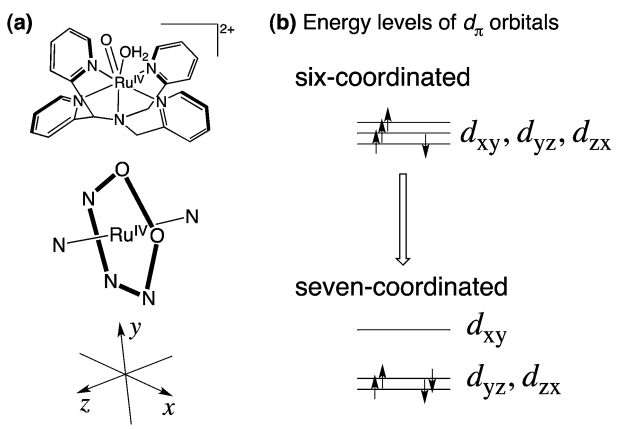


**Fig. 6** (a) Schematic description of a seven-coordinated structure of **6** and (b) the effect of the seven coordination on the energy levels of the $d_\pi$ orbitals.

In the case of oxidation of benzyl alcohol derivatives, the two-electron oxidation occurred to give the corresponding aldehydes for primary alcohols (entries 1–4) and the ketone for a secondary alcohol (entry 5). 1-Propanol underwent four-electron oxidation to afford propionic acid (entry 6) and 2-propanol was converted to acetone *via* two-electron oxidation (entry 7). Methanol with a C–H bond dissociation energy of 96.0 kcal $mol^{-1}$(ref. 34) could be oxidized to afford formaldehyde through two-electron oxidation (entry 8). Terminal and internal alkenes underwent oxidative C=C bond cleavage; styrene was converted to benzaldehyde (entry 9) and cyclohexene to adipic acid *via* an eight-electron oxidation (entry 10). A water-soluble ethylbenzene derivative was also converted to afford the acetophenone derivative *via* a four-electron oxidation (entry 11).

The oxidation efficiency for alcohols except methanol is nearly 100%, in common with all the three catalysts. On the other hand, the oxidation of olefins with catalyst **3** exhibited relatively low efficiencies compared to the catalysts **1** and **2**. The reason for the low efficiency is probably due to the difference in the stability among the three catalysts: the catalyst **1** is remarkably robust under catalytic conditions and alive even after more than 2500 catalytic cycles,[20a] whereas the catalyst **3** was not so stable and gradually decomposed under the same catalytic reaction conditions. Therefore, the oxidation of olefins, the rates of which were relatively slow as compared to those of alcohols, could not be completed by **3** because the catalyst **3** decomposed before the completion of the reaction.

### Kinetic studies under pseudo-first-order conditions

In order to reveal the reaction mechanisms of the oxidations of organic substrates with Ru(IV)-oxo complexes **4**–**6** and also to compare the reactivity among the three Ru(IV)-oxo complexes in the light of the difference of the spin states, we performed kinetic analyses on the quantitative oxidation of 1-propanol with electrochemically generated $Ru^{IV}$=O species **4**–**6**. The reactions were performed in the presence of an excess amount of 1-propanol (25–150 mM) relative to the $Ru^{IV}$=O species (0.5 mM) in B.–R. buffer and the rate constants were determined by monitoring absorbance changes at 624 nm for **4**, 628 nm for **5** and 440 nm for **6** at various temperatures (Fig. S13 in ESI†). All the time courses of the absorbance changes obeyed first-order kinetics and the pseudo-first-order rate constants were determined with various concentrations of 1-propanol (Fig. 7 and S14 in ESI†). In the oxidation of 1-propanol with **4**–**6**, saturation behaviors of the pseudo-first-order rate constants ($k_{obs}$) with respect to concentration of 1-propanol were commonly observed for **4**–**6** at all the temperatures examined, indicating the existence of pre-equilibrium processes prior to the oxidation. Hence, non-covalent interaction between 1-propanol and **4**–**6** results in formation of the corresponding precursor complexes. The curve fitting to the plots of $k_{obs}$ relative to concentration of the

**Table 2** Summary of turnover numbers and the oxidation efficiency (%) of the catalytic oxidation reactions with **1–3** as catalysts[a]

| | | | Turnover number[b] (efficiency, %) | | |
|---|---|---|---|---|---|
| | | | Catalyst | | |
| Entry | Substrate | Product | **1** | **2** | **3** |
| 1 | 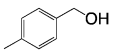 | 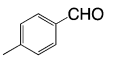 | 100 (100) | 100 (100) | 100 (100) |
| 2 | 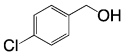 | 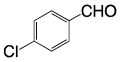 | 100 (100) | 98 (98) | 95 (95) |
| 3 | 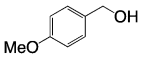 | 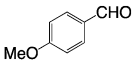 | 98 (98) | 96 (96) | 91 (91) |
| 4 |  |  | 93 (93) | 91 (91) | 90 (90) |
| 5 |  |  | 90 (90) | 88 (88) | 85 (85) |
| 6 |  |  | 50 (100) | 47 (94) | 42 (84) |
| 7 |  |  | 100 (100) | 98 (98) | 82 (82) |
| 8 | $CH_3OH$ | HCHO | 25 (25) | 23 (23) | 22 (22) |
| 9 |  |  | 46 (92) | 42 (84) | 39 (78) |
| 10 |  | 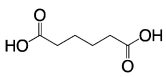 | 25 (100) | 23 (92) | 9 (36) |
| 11 | 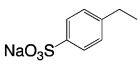 | 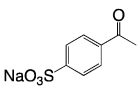 | 38 (76) | 35 (70) | 33 (66) |

[a] [Substrate] = 0.1 M, [CAN] = 0.2 M, [catalyst] = 1 μM. [b] Turnover number = [product]/[catalyst]; efficiency (%) = [product] × *n*/[CAN] (*n*: number of electrons related to the oxidation).

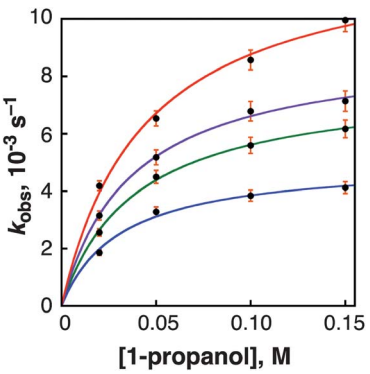


**Fig. 7** Pseudo-first-order kinetic analysis for the oxidation of 1-propanol with complex **6** as oxidant (0.5 mM) in B.–R. buffer (pH 1.8) at 308 (red), 301 (purple), 288 (green), and 280 K (blue).

substrate with eqn (1) gave the equilibrium constants ($K$) of the pre-equilibrium processes and the rate constants ($k$) of the oxidation reactions[35] and those values obtained at various temperatures are summarized in Table 3. The plots of the equilibrium constants $K$ and the rate constants $k$ relative to the inverse of the reaction temperatures ($T^{-1}$) (van't Hoff plots and Eyring plots, respectively; see Fig. S15 in ESI†) allowed us to obtain the thermodynamic parameters for the pre-equilibrium processes and the activation parameters for the oxidation reactions, respectively (Table 3).[36]

$$k_{obs} = kK[\text{1-propanol}]/(1 + K[\text{1-propanol}]) \quad (1)$$

As indicated by the thermodynamic parameters for the pre-equilibrium processes ($\Delta H$ and $\Delta S$), the formation of the precursor complexes is exothermic and the order of the $\Delta H$ values suggests that the interaction between 1-propanol and the $Ru^{IV}$=O complexes can be ascribed to the hydrogen bonding. In the hydrogen bonding, the aqua ligand of **4** and the additional aqua ligands of **5** and **6** affording a seven-coordination environment should play an important role in stabilizing the adduct between the oxo complexes and the substrate (*vide supra*). The activation parameters determined from the Eyring plots shed light on the transition states of the oxidation reactions and provide some fundamentals to consider the difference in the reactivities of **4–6**. The activation parameters obtained here for oxidants **4–6** are similar to each other, indicating that the reaction proceeds *via* similar transition states for the three oxidants in

 

**Table 3** Kinetic data for oxidation reactions with complexes **4–6**. (a) Equilibrium constants of adduct formation between the oxidant and 1-propanol and the thermodynamic parameters; (b) pseudo-first-order rate constants and the activation parameters for oxidation of 1-propanol at various temperatures; (c) equilibrium constants of the adduct formation and pseudo-first-order rate constants for oxidation of sodium 4-ethylbenzene sulfonate at 295 K

| (a) | **4** | **5** | **6** |
|---|---|---|---|
| $K_{308K}$ [$M^{-1}$] | 32 ± 5 | 27 ± 2 | 22 ± 3 |
| $K_{301K}$ [$M^{-1}$] | 36 ± 5 | 41 ± 2 | 28 ± 2 |
| $K_{288K}$ [$M^{-1}$] | 53 ± 3 | 61 ± 7 | 31 ± 2 |
| $K_{280K}$ [$M^{-1}$] | 92 ± 6 | 92 ± 4 | 45 ± 5 |
| $\Delta H$ [kJ $mol^{-1}$] | −23.8 ± 0.2 | −29.7 ± 0.3 | −16.2 ± 0.8 |
| $\Delta S$ [J $K^{-1}$ $mol^{-1}$] | −4.8 ± 0.3 | −6.8 ± 0.2 | −2.6 ± 0.1 |
| (b) | **4** | **5** | **6** |
| $k_{308K}$ [$10^{-3}$ $s^{-1}$] | 9.3 ± 0.4 | 8.2 ± 0.5 | 12.4 ± 0.5 |
| $k_{301K}$ [$10^{-3}$ $s^{-1}$] | 6.9 ± 0.3 | 5.2 ± 0.5 | 9.0 ± 0.2 |
| $k_{288K}$ [$10^{-3}$ $s^{-1}$] | 4.6 ± 0.3 | 3.7 ± 0.1 | 7.8 ± 0.2 |
| $k_{280K}$ [$10^{-3}$ $s^{-1}$] | 2.9 ± 0.5 | 2.6 ± 0.1 | 5.0 ± 0.2 |
| $\Delta H^{\ddagger}$ [kJ $mol^{-1}$] | 25.6 ± 0.4 | 22.0 ± 0.2 | 17.5 ± 0.8 |
| $\Delta S^{\ddagger}$ [J $K^{-1}$ $mol^{-1}$] | −201 ± 3 | −215 ± 2 | −225 ± 10 |
| (c) | **4** | **5** | **6** |
| $K_{295K}$ [$M^{-1}$] | 7.8 ± 1.0 | 7.8 ± 1.3 | 7.8 ± 1.9 |
| $k_{295K}$ [$10^{-3}$ $s^{-1}$] | 17.7 ± 1.0 | 15.8 ± 1.2 | 15 ± 2 |

terms of energies and structures. In addition, the negatively large activation entropies suggest the tight interaction between the substrate and the oxidants during the dehydrogenation processes (*vide infra*). The kinetic analysis was also conducted for the oxidation of sodium 4-ethylbenzene sulfonate (EBS) with oxidants **4–6** in water at 295 K. Unexpectedly, the pseudo-first-order rate constants ($k_{obs}$) exhibited saturation behavior relative to the concentration of EBS, which has no hydroxy group, in common for all the three oxidants (Fig. S16 in ESI†). The obtained pre-equilibrium constants and the rate constants for the oxidation of EBS at 295 K with **4–6** are summarized in Table 3c. The equilibrium constants of the precursor complex formation between the oxidant and the substrate in the oxidation of EBS are smaller than those for the oxidation of 1-propanol, whereas the rate constants of the former are larger than the latter. As EBS does not possess any strong hydrogen-bonding sites, the pre-equilibrium processes are possibly derived from weak non-covalent interactions between the substrate and the oxidants such as non-classical hydrogen bonding between the rather basic oxo ligand and the substrate C–H bond.[37] In addition, the larger rate constants for the oxidation of EBS compared to those for the oxidation of 1-propanol can be ascribed to the feasibility of the hydrogen atom abstraction from EBS than that from 1-propanol, as can be predicted from the values of bond dissociation energies (BDEs) of C–H bonds: 84.6 kcal $mol^{-1}$ for ethylbenzene and 93.7 kcal $mol^{-1}$ for 1-propanol.[34]

### Kinetic isotope effects on the oxidation of methanol

In order to obtain further information on the oxidation process, studies of the kinetic isotope effects (KIE) with the three $Ru^{IV}$=O complexes were conducted for the oxidation of methanol at 297 K. The KIE values were determined as the ratio of the rate constants ($k_H/k_D$) for the oxidation reactions of $CH_3OH$ and deuterated methanol derivatives (Fig. 8 and S17 in ESI†). The oxidation of $CH_3OH$ was performed in water in the presence of one of the three oxidants (**4–6**) (0.5 mM). $CD_3OH$ was formed *in situ* by addition of $CD_3OD$ (deuteration percentage: 99.8%) into the solution of one of the three oxidants in $H_2O$. The oxidation of $CH_3OD$ with one of the three oxidants was performed in a $D_2O$ solution of $CH_3OH$ (deuteration percentage: 99.9%). The reactions were monitored by UV-Vis spectroscopy to track the rise of the absorbance due to the $Ru^{II}$ species formed.

The pseudo-first-order rate constants for the methanol oxidation also displayed saturation behavior as in the cases of 1-propanol and EBS described above. The equilibrium constants and the first-order rate constants are summarized in Table 4. The pre-equilibrium constants are larger in the cases of oxidation of $CD_3OH$ in comparison with those of $CH_3OH$ for all the three oxidants; however, those for $CH_3OD$ were comparable to those for $CH_3OH$. The KIE values for the hydroxy group, which were determined by using $CH_3OH$ and $CH_3OD$ as substrates, were negligible for the three oxidants to be 1.0 for **4** and 1.1 for **5** and **6** (Table 4). In contrast, the oxidation of $CD_3OH$ was clearly retarded as compared to that of $CH_3OH$ to show KIE values to be 2.5 for **4**, 2.3 for **5**, and 1.7 for **6** (Table 4). The KIE values of $CH_3OD$ *vs.* $CD_3OH$ indicate that the hydrogen abstraction from the methyl group is involved in the rate-determining step, however, the hydrogen abstraction from the OH group is not involved in the rate-determining step.

The α-C–H bond in a hydrogen-bonded alcohol can be oriented to the oxo ligand to undergo hydrogen atom abstraction to give rise to a tightly condensed transition state, as reflected in the negatively large entropy ($\Delta S^{\ddagger}$), −201 ± 3 J $K^{-1}$ $mol^{-1}$ for **4**, −215 ± 2 J $K^{-1}$ $mol^{-1}$ for **5**, and −225 ± 10 J $K^{-1}$ $mol^{-1}$ for **6**, as given in Table 3. These data lend credence to the formation of a hydrogen-bonded and well-organized transition state as presented in Fig. 9.

### Reactivity of Ru(IV)-oxo complexes with different spin states

In light of the kinetic parameters listed in Tables 3 and 4, no significant difference in the reactivity was recognized among the

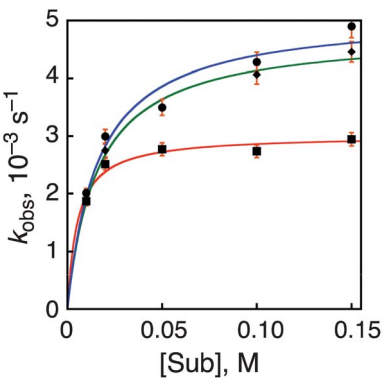


**Fig. 8** Pseudo-first-order kinetic analysis for oxidation reactions of $CH_3OH$ (blue line), $CD_3OH$ (red line) and $CH_3OD$ (green line) with complex **6** as oxidant at 297 K. $CH_3OH$ and the deuterated derivatives ($CD_3OH$ and $CH_3OD$) were used as substrates.

**Table 4** Rate constants and equilibrium constants for the oxidation of methanol with **4–6** at 297 K

| | **4** | **5** | **6** |
|---|---|---|---|
| $k_{CH_3OH}$ [$10^{-3}$ $s^{-1}$] | 5.0 ± 0.3 | 4.5 ± 0.3 | 5.1 ± 0.3 |
| $K_{CH_3OH}$ [$M^{-1}$] | 44 ± 6 | 43 ± 7 | 62 ± 15 |
| $k_{CD_3OH}$ [$10^{-3}$ $s^{-1}$] | 2.0 ± 0.6 | 2.0 ± 1.0 | 3.0 ± 0.1 |
| $K_{CD_3OH}$ [$M^{-1}$] | 43 ± 4 | 47 ± 9 | 96 ± 19 |
| $k_{CH_3OD}$ [$10^{-3}$ $s^{-1}$] | 5.0 ± 0.3 | 4.1 ± 0.2 | 4.8 ± 0.1 |
| $K_{CH_3OD}$ [$M^{-1}$] | 32 ± 3 | 41 ± 5 | 63 ± 7 |
| $k_H/k_D$ for $CH_3$ | 2.5 | 2.3 | 1.7 |
| $k_H/k_D$ for OH | 1.0 | 1.1 | 1.1 |

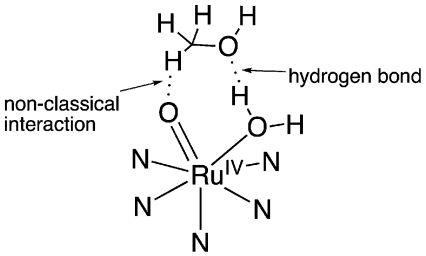


**Fig. 9** Plausible hydrogen bonding between seven-coordinate $Ru^{IV}$=O complexes with an aqua ligand and methanol.

three kinds of $Ru^{IV}$=O oxidants showing different spin states for the substrate oxidation reactions. A slight change in the rate constants was observed in relation to the oxidizing ability of the Ru(IV)-oxo complexes: the rate constants of **4–6** show linear relationships with the one-electron reduction potentials of **4–6** as demonstrated in Fig. 10. This observation indicates that the slight difference in the reaction rates and the activation parameters is probably derived from the difference in the electron-accepting ability of the three $Ru^{IV}$=O complexes,[35] but not from the difference in the spin state. Recently, Fujii and co-workers have also revealed the relationship between the activation barriers for oxidation reactions with iron-oxo complexes and the

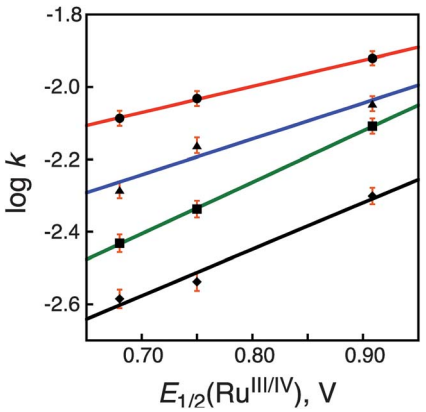


**Fig. 10** Plots of log $k$ for the oxidation of 1-propanol with $Ru^{IV}$=O complexes at various temperatures (at 308 K, filled circles and red line; at 301 K, filled triangles and blue line; at 288 K, filled squares and green line; at 280 K, filled rectangles and black line) *vs.* the one-electron reduction potentials of the $Ru^{IV}$=O complexes (+0.75 V for **4**, +0.68 V for **5**, +0.91 V for **6**). The one-electron reduction potentials *vs.* SCE were determined for 0.05 M solutions of **4–6** in B.–R. buffer (pH 1.8) at room temperature.

reduction potentials of the iron complexes.[38] So far, many examples have been examined to clarify the effects of difference in the spin state of the metal center on the reactivity of transition-metal complexes or organometallics.[39,40] As a consequence, it has been demonstrated that the high-spin state can exhibit higher reactivity than the spin isomer at the low-spin state.[39] As recently discussed by Mayer *et al.*,[41] however, the change in the reactivity may not be caused directly by the difference in the spin state, but by an indirect effect as a result of the difference in $\Delta G^\circ$ and/or reorganization energies of electron-transfer reactions. Thus, Mayer[41b] and de Visser[42] and their co-workers have indicated the important effects of the bond dissociation free-energy (BDFE) or bond dissociation enthalpy (BDE) of the metal-oxo complexes on the reactivity for the oxidation reactions.

### Mechanistic insight into hydrogen atom abstraction

Three possible reaction mechanisms can be considered for the H-atom abstraction from substrates: one-step hydride transfer as a two-electron oxidation step, electron transfer followed by proton transfer (ET/PT), and concerted proton-coupled electron transfer (PCET), in which a proton and an electron are transferred in a concerted manner.[43] Hydrogen atom transfer (HAT) reactions are also defined as the simultaneous transfer of an electron and proton between the same donor and acceptor.[44] However, PCET reactions typically involve different acceptors for the electron and proton,[45] as in the present case where an electron is transferred to the Ru(IV) center, but a proton is transferred to the oxo ligand of $Ru^{IV}$=O complexes. Because there is no significant difference in the reactivity between **1** with $S = 1$ and **2** and **3** with $S = 0$, the one-step hydride transfer, which is spin-forbidden for **1** to give the product at the singlet state, is unlikely to occur. The observation of the deuterium kinetic isotope effect (*vide supra*) and the small slope of the linear correlations between log $k$ and $E_{1/2}$ in Fig. 10 (0.7 at 308 K, 1.0 at 301 K, 1.4 at 288 K, and 1.3 at 280 K, respectively) indicate that the rate-determining step cannot be electron transfer. As pointed out by Hammarström and co-workers,[45] the rate constants of ET/PT should be much more sensitive to the driving forces ($\Delta G^\circ$) of electron-transfer reaction. Thus, a concerted PCET mechanism,[46–51] which is spin-allowed and irrespective of the spin states of the $Ru^{IV}$=O complexes and energetically favorable, must be dominant in the oxidation of substrates with the three oxidants **4–6**.

## Conclusion

We have synthesized a novel Ru(II)-aqua complex **3** and the corresponding $Ru^{IV}$=O complex **6** by using pentadentate N4Py as the auxiliary ligand and have determined the spin state of the $Ru^{IV}$ center in **6** to be the very rare $S = 0$. As suggested for **5** by DFT calculations,[20b] complex **6** could adopt a seven-coordinated structure with a solvent water molecule, and as a result, the low spin-state is energetically stabilized relative to the intermediate spin state ($S = 1$). We also employed other Ru(II)-aqua complexes **1** and **2** together with **3**, which bear similar pyridylamine coordination environments, as catalysts for oxidations of alcohols and olefins in the presence of CAN as an electron-transfer oxidant in an aqueous buffer solution to observe efficient and selective catalysis. Furthermore, the reactivity of the three

 

analogous $Ru^{IV}$=O complexes **4–6** in oxidation reactions was also scrutinized in the light of kinetic analyses on the oxidation reactions of organic substrates. As a result, the oxidation reaction was indicated to involve a pre-equilibrium process to form adducts between the Ru(IV)-oxo complexes and substrates through hydrogen bonding for alcohols and non-covalent interactions for EBS. Based on the activation parameters of the reactions and the kinetic isotope effect on the oxidation of methanol, it was clearly indicated that the slight difference in the reaction rates can be accounted for by the reduction potentials of the $Ru^{IV}$=O complexes and the spin states of the metal centers in the Ru(IV)-oxo complexes not influencing the reactivity. It was also clarified that the H-atom abstraction from substrates proceeded *via* a concerted PCET mechanism, in which a proton and an electron are transferred simultaneously from the substrate to the Ru(IV)-oxo complexes. Substrate oxidation is one of the most important chemical processes not only for the chemical industry but also for future energy production through artificial photosynthetic systems. The $Ru^{IV}$=O complexes presented here have exhibited one of the strongest oxidation reactivities in an energetically favorable PCET process involving a well-organized transition state. This work may provide a valuable basis to elucidate the reactivity of a high-valent metal-oxo complex in oxidation reactions of organic molecules, especially in those involving C–H bond functionalization.

## Experimental section

### General

Chemicals and solvents were used as received from Tokyo Chemical Industry (TCI) Co., Wako Chemicals, or Sigma-Aldrich Corp. unless otherwise mentioned. Synthetic details are described in the ESI.† $(NH_4)_2[Ce^{IV}(NO_3)_6]$ (CAN) was used as received and its purity was determined to be 95% by iodometry (see ESI†). UV-Vis spectra were obtained on a Shimadzu UV-3600 spectrophotometer, equipped with a UNISOK cryostat system, Unispecs. $^1$H NMR spectra were recorded on a JEOL EX-270 spectrometer in $D_2O$ (deuteration percentage: 99.9%) at room temperature and the chemical shift of each signal was determined relative to DSS (4,4-dimethyl-4-silapentane-1-sulfonic acid) as an internal reference. ESI-MS spectra were recorded on a JEOL AccuTOF CS JMS-T100CS mass spectrometer. Electrochemical measurements were performed on a BAS CV-1B voltammetric analyzer and an AUTOLAB PGSTAT12 potentiometer in Britton–Robinson (B.–R.) buffer (pH = 1.8–12)[27] at room temperature with a platinum disk as a working electrode, a platinum wire as a counter electrode, and $Ag/AgNO_3$ as a reference electrode. The raw potential was converted to those relative to SCE as 0 V by adding 0.29 V. Measurements of pH values were performed on a Horiba F-51 pH meter. Sample solutions of **6** for resonance Raman spectroscopic measurements were prepared with a 2 mM $H_2{}^{16}O$ or $H_2{}^{18}O$ solution of **3** (50 μL), which was oxidized by addition of a 20 mM aqueous solution of CAN (20 μL).

### Electrochemical generation of 4–6

A platinum mesh and a platinum wire employed as a working electrode and a counter electrode, respectively, were polished with 3 M $HNO_3$ (aq.) and rinsed well with water and dried before use. A silver wire was electrochemically oxidized in 0.1 M HCl (aq.) to generate an AgCl thin layer on the surface, which reached to 1 cm high from the tip of the wire. The Ag/AgCl wire was used as a reference electrode. These three electrodes were immersed in 0.5 mM sample solutions in B.–R. buffer (2 mL) in an electrochemical vessel equipped with an optical cell of 2 mm optical path length.[27] To this electrochemical system was loaded +1.3 V (*vs.* Ag/AgCl) potentiostatic voltage for 60 min with use of an AUTOLAB PGSTAT12 potentiometer, and the process of the reaction was monitored by UV-Vis spectroscopy.

### General procedures for catalytic oxidation reactions of organic substrates

A substrate (0.1 M) is dissolved in $D_2O$ (deuteration percentage: 99.9%) in the presence of a catalyst (**1**, **2** or **3**) (1 μM) and DSS (4 mM) as an internal standard to determine the chemical shifts and also to quantify the substrate and the product. Before adding an oxidant, the $^1$H NMR spectrum of the solution was measured. After adding CAN (0.2 M) to the solution, the solution was stirred for 1 h at 23 °C and then the $^1$H NMR spectrum of the resulting solution was measured to determine the yield of the oxidation product. The catalytic oxidation of *p*-methylbenzyl alcohol with each catalyst was done three times to check the reproducibility. For other substrates, the experiments were done one time with each catalyst.

### Kinetic studies on oxidation reactions with $Ru^{IV}$=O species

The $Ru^{IV}$=O species, **4**, **5** and **6** (0.5 mM) were generated in B.–R. buffer (pH 1.8) from the corresponding $Ru^{II}$-aqua complexes **1**, **2** and **3**, respectively, through bulk electrolysis as mentioned above. To the solution of the $Ru^{IV}$=O complex generated, was added a substrate (1-propanol, sodium 4-ethylbenzenesulfonate, methanol and the deuterated derivatives) with various concentrations and at various temperatures. The reaction profiles were monitored by the rise of the absorption assigned to the resulting $Ru^{II}$–$OH_2$ complex at 620 nm for **4**, 630 nm for **5**, and 440 nm for **6**. The error bars (drawn as hammer-shaped orange lines) in figures for the kinetic studies and standard deviations of the kinetic and thermodynamic parameters in tables were estimated with accuracy values of the fitting curves.

## Acknowledgements

This work was supported by Grants-in-Aid (no. 20108010, 21350035, 22245028, and 24245011), a Global COE program, "the Global Education and Research Center for Bio-Environmental Chemistry" from the Japan Society of Promotion of Science (JSPS, MEXT) of Japan, and by KOSEF/MEST through WCU project (R31-2008-000-10010-0) of Korea. T. K. also appreciates financial support from The Asahi Glass Foundation and The Iwatani Naoji Foundation.

## Notes and references

1 (*a*) R. A. Sheldon and J. K. Kochi, *Metal-Catalyzed Oxidations of Organic Compounds*, Academic Press, New York, 1981; (*b*) W. A. Nugent and J. M. Mayer, *Metal–Ligand Multiple Bonds*, Wiley, New York, 1988; (*c*) B. Meunier, *Biomimetic Oxidations*

*Catalyzed by Transition Metal Complexes*, Imperial College Press, London, 1998; (*d*) T. Punniyamurthy, S. Velusamy and J. Iqbal, *Chem. Rev.*, 2005, **105**, 2329.
2 (*a*) P. R. Ortiz de Montellano, *Cytochrome P450: Structure Mechanism, and Biochemistry*, Kluwer Academic/Plenum, New York, 3rd edn, 2004; (*b*) B. Meunier, S. P. de Visser and S. Shaik, *Chem. Rev.*, 2004, **104**, 3947; (*c*) I. G. Denisov, T. M. Makris, S. G. Sligar and I. Schlichting, *Chem. Rev.*, 2005, **105**, 2253–2278.
3 (*a*) R. H. Holm, *Chem. Rev.*, 1987, **87**, 1401; (*b*) A. E. Shilov and G. B. Shul'pin, *Chem. Rev.*, 1997, **97**, 2879; (*c*) D. Balcells, E. Clot and O. Eisenstein, *Chem. Rev.*, 2010, **110**, 749; (*d*) A. Gunay and K. H. Theopold, *Chem. Rev.*, 2010, **110**, 1060.
4 (*a*) L. Que, Jr and R. Y. N. Ho, *Chem. Rev.*, 1996, **96**, 2607; (*b*) M. Costas, M. P. Mehn, M. P. Jensen and L. Que, Jr, *Chem. Rev.*, 2004, **104**, 939; (*c*) M. M. Abu-Omar, A. Loaiza and N. Hontzeas, *Chem. Rev.*, 2005, **105**, 2227; (*d*) J. A. Kovacs, *Science*, 2009, **299**, 1024.
5 (*a*) S. J. Lange, H. Miyake and L. Que, Jr, *J. Am. Chem. Soc.*, 1999, **121**, 6330; (*b*) N. Lehnert, R. Y. N. Ho, L. Que, Jr and E. I. Solomon, *J. Am. Chem. Soc.*, 2001, **123**, 8271; (*c*) J. Kaizer, E. J. Klinker, N. Y. Oh, J.-U. Rohde, W. J. Song, A. Stubna, J. Kim, E. Münck, W. Nam and L. Que, Jr, *J. Am. Chem. Soc.*, 2004, **126**, 472; (*d*) Y. Morimoto, H. Kotani, J. Park, Y.-M. Lee, W. Nam and S. Fukuzumi, *J. Am. Chem. Soc.*, 2011, **133**, 403; (*e*) J. Park, Y. Morimoto, Y.-M. Lee, W. Nam and S. Fukuzumi, *J. Am. Chem. Soc.*, 2011, **133**, 5236; (*f*) J. Park, Y. Morimoto, Y.-M. Lee, W. Nam and S. Fukuzumi, *J. Am. Chem. Soc.*, 2012, **134**, 3903.
6 (*a*) J.-U. Rohde, J.-H. In, M. H. Lim, W. W. Brennessel, M. R. Bukowski, A. Stubna, E. Münck, W. Nam and L. Que, Jr, *Science*, 2003, **299**, 1037; (*b*) C. E. MacBeth, R. Gupta, K. R. Mitchell-Koch, V. G. Young, Jr, G. H. Lushington, W. H. Thompson, M. P. Hendrich and A. S. Borovik, *J. Am. Chem. Soc.*, 2004, **126**, 2556; (*c*) S. Fukuzumi, Y. Morimoto, H. Kotani, P. Naumov, Y.-M. Lee and W. Nam, *Nat. Chem.*, 2010, **2**, 756; (*d*) D. C. Lacy, R. Gupta, K. L. Stone, J. Greaves, J. W. Ziller, M. P. Hendrich and A. S. Borovik, *J. Am. Chem. Soc.*, 2010, **132**, 12188.
7 (*a*) Z. Shirin, B. S. Hammes, V. G. Young, Jr and A. S. Borovik, *J. Am. Chem. Soc.*, 2000, **122**, 1836; (*b*) G. Yin, M. Buchalova, A. M. Danby, C. M. Perkins, D. Kitko, J. D. Carter, W. M. Scheper and D. H. Busch, *J. Am. Chem. Soc.*, 2005, **127**, 17170; (*c*) G. Yin, A. M. Danby, D. Kitko, J. D. Carter, W. M. Scheper and D. H. Busch, *J. Am. Chem. Soc.*, 2008, **130**, 16245; (*d*) S. Fukuzumi, N. Fujioka, H. Kotani, K. Ohkubo, Y.-M. Lee and W. Nam, *J. Am. Chem. Soc.*, 2009, **131**, 17127; (*e*) S. H. Kim, H. Park, M. S. Seo, M. Kubo, T. Ogura, J. Klajn, D. T. Gryko, J. S. Valentine and W. Nam, *J. Am. Chem. Soc.*, 2010, **132**, 14030.
8 J. D. Blakemore, N. D. Schley, D. Balcells, J. F. Hull, G. W. Olack, C. D. Incarvito, O. Eisenstein, G. W. Brudvig and R. H. Crabtree, *J. Am. Chem. Soc.*, 2010, **132**, 16017.
9 T. M. Anderson, W. A. Neiwert, M. L. Kirk, P. M. B. Piccoli, A. J. Schultz, T. F. Koetzle, D. G. Musaev, K. Morokuma, R. Cao and C. L. Hill, *Science*, 2004, **306**, 2074.
10 (*a*) B. T. Farrer, J. S. Pickett and H. H. Thorp, *J. Am. Chem. Soc.*, 2000, **122**, 549; (*b*) W. W. Y. Lam, W.-L. Man, C.-F. Leung, C.-Y. Wong and T.-C. Lau, *J. Am. Chem. Soc.*, 2007, **129**, 13646.
11 (*a*) M. H. V. Huynh and T. J. Meyer, *Chem. Rev.*, 2007, **107**, 5004; (*b*) V. R. I. Kaila, M. Verkhovsky and M. Wikström, *Chem. Rev.*, 2010, **110**, 7062; (*c*) J. J. Warren, T. A. Tronic and J. M. Mayer, *Chem. Rev.*, 2010, **110**, 6961; (*d*) C. J. Gagliardi, B. C. Westlake, C. A. Kent, J. J. Paul, J. M. Papanikolas and T. J. Meyer, *Coord. Chem. Rev.*, 2010, **254**, 2459.
12 (*a*) H. Kotani, T. Suenobu, Y.-M. Lee, W. Nam and S. Fukuzumi, *J. Am. Chem. Soc.*, 2011, **133**, 3249; (*b*) S. Fukuzumi, T. Kishi, H. Kotani, Y.-M. Lee and W. Nam, *Nat. Chem.*, 2011, **3**, 38.
13 (*a*) W. Rüttinger and G. C. Dismukes, *Chem. Rev.*, 1997, **97**, 1; (*b*) J. P. McEvoy and G. W. Brudvig, *Chem. Rev.*, 2006, **106**, 4455; (*c*) T. J. Meyer, M. H. V. Huynh and H. H. Thorp, *Angew. Chem., Int. Ed.*, 2007, **46**, 5284.
14 (*a*) K. N. Ferreira, T. M. Iverson, K. Maghlaoui, J. Barber and S. Iwata, *Science*, 2004, **303**, 1831; (*b*) Y. Umena, K. Kawakami, J.-R. Shen and N. Kamiya, *Nature*, 2011, **473**, 55.
15 (*a*) M. S. Thompson and T. J. Meyer, *J. Am. Chem. Soc.*, 1982, **104**, 4106; (*b*) R. A. Binstead, M. E. McGuire, A. Dovletoglou, W. K. Seok, L. E. Roecker and T. J. Meyer, *J. Am. Chem. Soc.*, 1992, **114**, 173; (*c*) E. L. Lebeau and T. J. Meyer, *Inorg. Chem.*, 1999, **38**, 2174; (*d*) R. A. Binstead, C. W. Chronister, J. Ni, C. M. Hartshorn and T. J. Meyer, *J. Am. Chem. Soc.*, 2000, **122**, 8464; (*e*) J. J. Concepcion, M.-K. Tsai, J. T. Muckerman and T. J. Meyer, *J. Am. Chem. Soc.*, 2010, **132**, 1545.
16 (*a*) A. Sartorel, P. Miró, E. Salvadori, S. Romain, M. Carraro, G. Scorrano, M. Di Valentin, A. Llobet, C. Bo and M. Bonchio, *J. Am. Chem. Soc.*, 2009, **131**, 16051; (*b*) A. Sartorel, M. Carraro, G. Scorrano, R. De Zorzi, S. Geremia, N. D. McDaniel, S. Bernhard and M. Bonchio, *J. Am. Chem. Soc.*, 2008, **130**, 5006; (*c*) M. Murakami, D. Hong, T. Suenobu, S. Yamaguchi, T. Ogura and S. Fukuzumi, *J. Am. Chem. Soc.*, 2011, **133**, 11605.
17 (*a*) Y. V. Geletii, C. Besson, Y. Hou, Q. Yin, D. G. Musaev, D. Quiñonero, R. Cao, K. I. Hardcastle, A. Proust, P. Kögerler and C. L. Hill, *J. Am. Chem. Soc.*, 2009, **131**, 17360; (*b*) A. E. Kuznetsov, Y. V. Geletii, C. L. Hill, K. Morokuma and D. G. Musaev, *J. Am. Chem. Soc.*, 2009, **131**, 6844; (*c*) Y. V. Geletii, B. Botar, P. Kögerler, D. A. Hillesheim, D. G. Musaev and C. L. Hill, *Angew. Chem., Int. Ed.*, 2008, **47**, 3896.
18 (*a*) F. Bozoglian, S. Romain, M. Z. Ertem, T. K. Todorova, C. Sens, J. Mola, M. Rodríguez, I. Romero, J. Benet-Buchholz, X. Fontrodona, C. J. Cramer, L. Gagliardi and A. Llobet, *J. Am. Chem. Soc.*, 2009, **131**, 15176; (*b*) S. Romain, F. Bozoglian, X. Sala and A. Llobet, *J. Am. Chem. Soc.*, 2009, **131**, 2768.
19 (*a*) W. K. Seok and T. J. Meyer, *J. Am. Chem. Soc.*, 1988, **110**, 7358; (*b*) A. Paul, J. F. Hull, M. R. Norris, Z. Chen, D. H. Ess, J. J. Concepcion and T. J. Meyer, *Inorg. Chem.*, 2011, **50**, 1167.
20 (*a*) Y. Hirai, T. Kojima, Y. Mizutani, Y. Shiota, K. Yoshizawa and S. Fukuzumi, *Angew. Chem., Int. Ed.*, 2008, **47**, 5772; (*b*) T. Kojima, Y. Hirai, T. Ishizuka, Y. Shiota, K. Yoshizawa, K. Ikemura, T. Ogura and S. Fukuzumi, *Angew. Chem., Int. Ed.*, 2010, **49**, 8449.
21 (*a*) D. Schröder and S. Shaik, *Angew. Chem., Int. Ed.*, 2011, **50**, 3850; (*b*) T. Kojima and S. Fukuzumi, *Angew. Chem., Int. Ed.*, 2011, **50**, 3852.
22 M. Lubben, A. Meetsma, E. C. Wilkinson, B. Feringa and L. Que, Jr, *Angew. Chem., Int. Ed. Engl.*, 1995, **34**, 1512.
23 (*a*) K. Shiren, S. Ogo, S. Fujinami, H. Hayashi, M. Suzuki, A. Uehara, Y. Watanabe and Y. Moro-oka, *J. Am. Chem. Soc.*, 2000, **122**, 254; (*b*) H. Hayashi, K. Uozumi, S. Fujinami, S. Nagatomo, K. Shiren, H. Furutachi, M. Suzuki, A. Uehara and T. Kitagawa, *Chem. Lett.*, 2002, 416; (*c*) D. G. Lonnon, D. C. Craig and S. B. Colbran, *Inorg. Chem. Commun.*, 2003, **6**, 1351; (*d*) M. Mizuno, K. Honda, J. Cho, H. Furutachi, T. Tosha, T. Matsumoto, S. Fujinami, T. Kitagawa and M. Suzuki, *Angew. Chem., Int. Ed.*, 2006, **45**, 6911.
24 T. Kojima, D. M. Weber and C. T. Choma, *Acta Crystallogr., Sect. E: Struct. Rep. Online*, 2005, **61**, m226.
25 A. G. Orpen, L. Brammer, F. A. Allen, O. Kennard and D. G. Watson, *J. Chem. Soc., Dalton Trans.*, 1989, S1.
26 (*a*) J. Benet-Buchholz, P. Comba, A. Llobet, S. Roeser, P. Vadivelu, H. Wadepohl and S. Wiesner, *Dalton Trans.*, 2009, 5910; (*b*) R. Zong, F. Naud, C. Segal, J. Burke, F. Wu and R. Thummel, *Inorg. Chem.*, 2004, **43**, 6195; (*c*) X.-J. Yang, F. Drepper, B. Wu, W.-H. Sun, W. Haehnel and C. Janiak, *Dalton Trans.*, 2005, 256; (*d*) N. Gupta, N. Grover, G. A. Neyhart, W. Liang, P. Singh and H. H. Thorp, *Angew. Chem., Int. Ed. Engl.*, 1992, **31**, 1048.
27 R. Wang, J. G. Vos, R. H. Schmehl and R. Hage, *J. Am. Chem. Soc.*, 1992, **114**, 1964.
28 In this experiment, the aqua-complex **3** was dissolved in 99%-enriched $H_2{}^{18}O$ and then oxidized with CAN into **6**, but as the substitution rate of the aqua ligand in **3** was slow, thus the enriched efficiency of **6** observed within the ESI MS spectrum was about 50%.
29 The Raman scatterings derived from the $Ru^{IV}$=O moiety in **6** and the $^{18}O$-derivative were very weak, because the Ru(IV)-oxo complex underwent facile photo-conversion to afford the corresponding aqua-complex **3** by the laser excitation at 353 nm. Details of the photo-conversion are currently under investigation.
30 T. Kojima, K. Nakayama, K. Ikemura, T. Ogura and S. Fukuzumi, *J. Am. Chem. Soc.*, 2011, **133**, 11692.
31 In this experiment, 10 mol equiv. of CAN was required despite the theoretical requirement being only 2 mol equiv. The reason may result from the relation between the stability of CAN and the solution pH. In fact, UV-Vis experiments indicated that 10 mol

 

equiv. CAN was required to fully oxidize **3** into **6** in neutral water, whereas the reaction was completed with addition of 2 mol equiv. of CAN in B.–R. buffer (pH 1.8) (Fig. S8 in ESI†).
32 The assignment of the $^1$H NMR signals of the pyridine rings was made using a differential NOE spectrum of complex **6** in $D_2O$. The signal due to 3-H of the N2- and N3-pyridine rings at 9.00 ppm showed a correlation with the signal assigned to the methine proton at 7.41 ppm (Fig. S10 in ESI†).
33 Experimental details of the control experiments are described in the ESI† and the $^1$H NMR spectra of the selected examples for the oxidation reaction of the substrates with CAN only are shown in Fig. S12 in the ESI† with the oxidation efficiencies.
34 Y.-R. Luo, *Handbook of Bond Dissociation Energies in Organic Compounds*, CRC Press, Boca Raton, 2003.
35 (*a*) E. A. Mader, E. R. Davidson and J. M. Mayer, *J. Am. Chem. Soc.*, 2007, **129**, 5153; (*b*) W. W. Y. Lam, M. F. W. Lee and T.-C. Lau, *Inorg. Chem.*, 2006, **45**, 315.
36 The obtained rate constants and the activation parameters for **4** and **5** are slightly different from those given in previous reports (ref. 20*b*). Probably the reason is ascribed to the difference in the generation methods of the oxo species. In ref. 20*b*, the oxo complexes as active species were formed with addition of 2 mol equiv. of CAN in neutral water.
37 (*a*) I. Garcia-Bosch, A. Company, C. W. Cady, S. Styring, W. R. Browne, X. Ribas and M. Costas, *Angew. Chem., Int. Ed.*, 2011, **50**, 5648; (*b*) T. Steiner, *Angew. Chem., Int. Ed.*, 2002, **41**, 48.
38 A. Takahashi, D. Yamaki, K. Ikemura, T. Kurahashi, T. Ogura, M. Hada and H. Fujii, *Inorg. Chem.*, 2012, **51**, 7296.
39 (*a*) H. Hirao, D. Kumar, L. Que, Jr and S. Shaik, *J. Am. Chem. Soc.*, 2006, **128**, 8590; (*b*) S. N. Dhuri, M. S. Seo, Y.-M. Lee, H. Hirao, Y. Wang, W. Nam and S. Shaik, *Angew. Chem., Int. Ed.*, 2008, **47**, 3356; (*c*) E. J. Klinker, S. Shaik, H. Hirao and L. Que, Jr, *Angew. Chem., Int. Ed.*, 2009, **48**, 1291; (*d*) G. Q. Xue, R. De Hont, E. Munck and L. Que, Jr, *Nat. Chem.*, 2010, **2**, 400; (*e*) D. Janardanan, Y. Wang, P. Schyman, L. Que, Jr and S. Shaik, *Angew. Chem., Int. Ed.*, 2010, **49**, 3342; (*f*) M. S. Seo, N. H. Kim, K.-B. Cho, J. E. So, S. K. Park, M. Clemancey, R. Garcia-Serres, J.-M. Latour, S. Shaik and W. Nam, *Chem. Sci.*, 2011, **2**, 1039.
40 (*a*) J. L. Detrich, O. M. Reinaud, A. L. Rheingold and K. H. Theopold, *J. Am. Chem. Soc.*, 1995, **117**, 11745; (*b*) D. W. Keogh and R. Poli, *J. Am. Chem. Soc.*, 1997, **119**, 2516; (*c*) J. L. Carreón-Macedo and J. N. Harvey, *J. Am. Chem. Soc.*, 2004, **126**, 5789; (*d*) J. N. Harvey, P. Poli and K. M. Smith, *Coord. Chem. Rev.*, 2003, **238–239**, 347; (*e*) N. A. Eckert, S. Vaddadi, S. Stoian, R. J. Lachicotte, T. R. Cundari and P. L. Holland, *Angew. Chem., Int. Ed.*, 2006, **45**, 6868.
41 (*a*) J. C. Yoder, J. P. Roth, E. M. Gussenhoven, A. S. Larsen and J. M. Mayer, *J. Am. Chem. Soc.*, 2003, **125**, 2629; (*b*) J. M. Mayer, *Acc. Chem. Res.*, 2011, **44**, 36.
42 D. Kumar, B. Karamzadeh, G. N. Sastry and S. P. de Visser, *J. Am. Chem. Soc.*, 2010, **132**, 7656.
43 For the mechanistic border line between ET/PT and concerted PCET, see: (*a*) J. Yuasa and S. Fukuzumi, *J. Am. Chem. Soc.*, 2006, **128**, 14281; (*b*) S. Fukuzumi and H. Kotani, in *Proton-Coupled Electron Transfer*, RSC Catalysis Series No. 8, ed. S. Formoshinho and M. Barroso, RSC Publishing, Cambridge, 2012, pp. 89–125.
44 A. Sirjoosingh and S. Hammes-Schiffer, *J. Phys. Chem. A*, 2011, **115**, 2367.
45 (*a*) M. Sjödin, S. Styring, H. Wolpher, Y. Xu, L. Sun and L. Hammarström, *J. Am. Chem. Soc.*, 2005, **127**, 3855; (*b*) A. A. Zieba, C. Richardson, C. Lucero, S. D. Dieng, Y. M. Gindt and J. P. M. Schelvis, *J. Am. Chem. Soc.*, 2011, **133**, 7824.
46 E. A. Mader and J. M. Mayer, *Inorg. Chem.*, 2010, **49**, 3685.
47 (*a*) M. J. Knapp, K. W. Rickert and J. P. Klinman, *J. Am. Chem. Soc.*, 2002, **124**, 3865; (*b*) E. Hatcher, A. V. Soudackov and S. Hammes-Schiffer, *J. Am. Chem. Soc.*, 2007, **129**, 187; (*c*) M. P. Meyer and J. P. Klinman, *Chem. Phys.*, 2005, **319**, 283; (*d*) M. K. Ludlow, A. V. Soudackov and S. Hammes-Schiffer, *J. Am. Chem. Soc.*, 2009, **131**, 7094.
48 C. J. Fecenko, H. H. Thorp and T. J. Meyer, *J. Am. Chem. Soc.*, 2007, **129**, 15098.
49 (*a*) M. Sjödin, S. Styring, B. Åkermark, L. Sun and L. Hammarström, *J. Am. Chem. Soc.*, 2000, **122**, 3932; (*b*) M. K. Ludlow, A. V. Soudackov and S. Hammes-Schiffer, *J. Am. Chem. Soc.*, 2009, **131**, 7094.
50 (*a*) R. A. Binstead, M. F. McGuire, A. Dovletglou, W. K. Seok, L. E. Roecker and T. J. Meyer, *J. Am. Chem. Soc.*, 1992, **114**, 173; (*b*) E. L. Lebeau, R. A. Binstead and T. J. Meyer, *J. Am. Chem. Soc.*, 2001, **123**, 10535; (*c*) M. H. V. Huynh and T. J. Meyer, *Angew. Chem., Int. Ed.*, 2002, **41**, 1395.
51 S. Hammes-Schiffer, *Acc. Chem. Res.*, 2009, **42**, 1881.